Structural and Biochemical Characterization of CIB1 Delineates a New Family of EF-hand-containing Proteins*

Holly R. Gentry‡§¶¶, Alex U. Singer‡§, Laurie Betts‡, Cheng Yang¶, Joseph D. Ferrara¶, John Sondek‡∥‡‡, and Leslie V. Parise‡**§§**

*From the ‡Department of Pharmacology, the §§Carolina Cardiovascular Biology Center, the ∥Department of Biochemistry and Biophysics, and the **Lineberger Comprehensive Cancer Center, The University of North Carolina, Chapel Hill, North Carolina 27599-7365 and ¶Rigaku/MSC Inc., The Woodlands, Texas 77381*

CIB1 (CIB) is an EF-hand-containing protein that binds multiple effector proteins, including the platelet αIIbβ3 integrin and several serine/threonine kinases and potentially modulates their function. The crystal structure for Ca^{2+}-bound CIB1 has been determined at 2.0 Å resolution and reveals a compact α-helical protein containing four EF-hands, the last two of which bind calcium ions in the standard fashion seen in many other EF-hand proteins. CIB1 shares high structural similarity with calcineurin B and the neuronal calcium sensor (NCS) family of EF-hand-containing proteins. Most importantly, like calcineurin B and NCS proteins, which possess a large hydrophobic pocket necessary for ligand binding, CIB1 contains a hydrophobic pocket that has been implicated in ligand binding by previous mutational analysis. However, unlike several NCS proteins, Ca^{2+}-bound CIB1 is largely monomeric whether bound to a relevant peptide ligand or ligand-free. Differences in structure, oligomeric state, and phylogeny define a new family of CIB1-related proteins that extends from arthropods to humans.

One important mechanism by which cells respond to changes in Ca^{2+} levels involves the activation of EF-hand proteins, such as calmodulin. Upon Ca^{2+} binding, these proteins undergo structural changes that allow them to bind and activate target proteins. At least two specific structural changes can occur in EF-hand-containing proteins due to Ca^{2+} binding that facilitate signal transduction. The first type of change occurs when a hydrophobic binding pocket becomes accessible, thus facilitating ligand binding. The second type of change, termed a myristoyl switch, involves the extrusion of an N-terminal myristoyl group from a hydrophobic cavity in the protein, thereby leading to membrane localization, as described in recoverin (1) and related proteins.

Recoverin and related proteins are termed neuronal calcium sensors (NCS)[1] due to their neuronal expression pattern and high degree of homology (2). These proteins have a variety of functions; recoverin directly inhibits rhodopsin kinase (3), while a subgroup of NCS proteins that includes frequenin modulates synaptic activity, neurotransmitter release, and vesicle secretion (2). NCS proteins bind Ca^{2+} at levels just above basal Ca^{2+} concentrations and reach half maximal binding below 1 μM free Ca^{2+}, which is a 10-fold higher affinity than that of calmodulin (4). Therefore, these proteins are fully active at intracellular Ca^{2+} concentrations that activate only a small fraction of calmodulin.

CIB1 (CIB, calmyrin, and KIP) is an EF-hand-containing protein that possesses many features of NCS proteins. CIB1 contains four EF-hand domains (denoted EF1–4), two of which bind Ca^{2+} (EF3 and EF4) with affinities of 1.9 and 0.54 μM, respectively (5). These values are comparable to the Ca^{2+} affinities seen in NCS proteins. In addition, CIB1 is N-terminally myristoylated (6), although it is unknown whether it functions as a Ca^{2+}-myristoyl switch, despite sequence similarity in its myristoyl-binding pocket to the Ca^{2+}-myristoyl switch protein recoverin (7, 8). The myristoyl group of CIB1 may target it to membranes, since CIB1 fractionates exclusively with membrane fractions in both nucleated (6) and non-nucleated (9) cells. Moreover, disruption of myristoylation by addition of an N-terminal myc tag causes CIB1 staining to shift from membranes to a diffuse cytosolic and nuclear pattern (6). However, myristoylation does not appear to be required for CIB1 binding to its ligands (9, 10).

Unlike NCS proteins, CIB1 is not exclusively neuronal, but is widely expressed (9). Moreover, CIB1 is less homologous in sequence to several NCS proteins, such as KChIP1 (46%), neurocalcin (46%), and frequenin (43%) than they are to one another (2). In fact, CIB1 is more homologous to the EF-hand proteins calcineurin B (57% similarity) and calmodulin (54%). CIB1 was originally identified in a yeast two-hybrid screen as a binding partner for the cytoplasmic tail of the platelet integrin αIIb (11). Subsequently, additional CIB1-binding proteins were identified, including DNA-dependent protein kinase (12), the polo-like kinases Fnk and Snk (13), Rac3 (10), Pax3 (14), and presenilin 2 (6), and CIB1 has been shown to modify the function of some of these proteins (14, 15).

Integrins are heterodimeric cell adhesion receptors containing

[1] The abbreviations used are: NCS, neuronal calcium sensor; BTP, bis-Tris propane (1,3-bis[tris(hydroxymethyl)methylamino]propane); MES, 2-(*N*-morpholino)ethanesulfonic acid; AUC, analytical ultracentrifugation; r.m.s.d., root mean square deviation.

an α and β subunit that can exist in a resting conformation on unactivated cells and convert to an active conformation upon cell stimulation, resulting in a conformational change that allows the integrin to bind its adhesive protein ligands with higher affinity. The αIIbβ3 integrin is expressed only on platelets and their precursors, megakaryocytes, and is the most abundant integrin on these cells. CIB1 binding to αIIb appears to modulate the activation state of the integrin (16, 17), platelet spreading (18), and FAK activation (19). The CIB1 binding region of αIIb has been delineated, and corresponds to a membrane-proximal portion of the cytoplasmic tail, including several amino acids within the putative transmembrane domain (7). These binding residues of αIIb are likely to form an amphipathic α-helix (20, 21), which agrees with data showing that the hydrophobic crevices of EF-hand-containing proteins bind α-helical regions, such as the binding of calcineurin B to calcineurin A (22) and the binding of KChIP1 to the Kv4.2 channel (23).

The sequences of three CIB1 homologs (CIB2, -3, and -4) are also found in the human genome. CIB1 and some of its homologs have been identified in other vertebrates, and highly homologous sequences are present in the genome of more simple organisms such as *Drosophila melanogaster*. Sequence analysis indicates CIB1 and its homologs form a protein family distinct from those of the calcineurin B and the NCS families. To help determine the molecular mechanism for CIB1 binding to its various targets, we describe the x-ray crystal structure of Ca^{2+}-bound CIB1 to 2.0 Å.

<center>MATERIALS AND METHODS</center>

Protein Purification—Human wild type CIB1 and CIB1 Δ1–8 (residues 9–191), each fused to an N-terminal hexahistidine tag, were expressed from pProEX HTc (Invitrogen) in *Escherichia coli* BL21(DE3) cells. The final DNA sequence includes a hexahistidine Ni-affinity tag followed by a tobacco etch virus cleavage site at the N terminus; the tag was later removed from the protein as described below. CIB1 Δ1–8 was used for crystallization experiments. Wild-type CIB1 was used for gel filtration and analytical ultracentrifugation experiments.

Expression of CIB1 was initiated by inoculating 1 liter of LB broth with 100 ml of overnight culture and incubating at 37 °C. CIB1 expression was induced after 4 h by the addition of isopropyl 1-thio-β-D-galactopyranoside to a final concentration of 1 mM, and cells were incubated for an additional 3 h at 37 °C. Cells were centrifuged at $2000 \times g$ for 20 min and resuspended in Buffer A, composed of 20 mM Tris, 10 mM imidazole, 100 mM NaCl, 10% (v/v) glycerol, and 100 μM $CaCl_2$ (pH 7.5) with 1 tablet of "Complete EDTA-free protease inhibitor mixture" (Roche Applied Science). Cells were lysed by one pass through an EmulsiFlex-C5 (Avestin) homogenizer, and lysed cells were centrifuged at $200,000 \times g$ for 40 min. Clarified cell lysate was loaded onto two 5-ml Hi-Trap chelating HP columns in series (Amersham Biosciences) that had been preloaded with 100 mM $NiSO_4$ and equilibrated with buffer. The column was washed with 5 and 30% of Buffer B (Buffer A plus 1 M imidazole) and CIB1 was eluted at 40% of this buffer. Fractions containing CIB1 were pooled and dialyzed 1 h in 20 mM Tris, 10 mM NaCl, 10% (v/v) glycerol, and 100 μM $CaCl_2$ (pH 7.5) to dilute the imidazole and remove residual Ni^{2+}. Dialysis and removal of the His tag was performed by overnight incubation with 4 ml of tobacco etch virus (purified as stated previously (24)) in dialysis buffer that also contains 5 mM dithiothreitol. Analysis of the extent of cleavage was performed by analyzing samples by SDS-PAGE. If additional cleavage was required, further incubation with additional tobacco etch virus was performed. CIB1 was further purified by an S-200 gel filtration column (Amersham Biosciences) equilibrated with 20 mM Tris, 150 mM NaCl, and 5 mM dithiothreitol (pH 7.5). Fractions were analyzed by SDS-PAGE, and the purest fractions were concentrated using a Vivaspin 10 MWCO concentrator (Vivascience, Hannover, Germany), and the buffer was exchanged to 20 mM MES, pH 6.5, 10 mM NaCl, 2 mM dithiothreitol (pH 6.5) by several rounds of dilution and concentration. Protein was frozen in 50-μl aliquots at 30 mg/ml. Quantities of 40–50 mg of protein were obtained per liter of broth.

Crystallization—Crystals of purified CIB1 Δ1–8 were obtained by sitting drop vapor diffusion at 18 °C for 3–5 days by equilibrating against 20 mM Bis-Tris propane, 300 mM calcium acetate, and 18% polyethylene glycol 3350 (pH 6.8) and reached full size after 10 days.

Crystals were cryoprotected by slowly equilibrating the crystal drop to glycerol in increments of 2%, 4%, 6%, 8%, 10%, 15%, and 20% (v/v) glycerol in the mother liquor solution, followed by flash freezing in liquid nitrogen.

Gel Filtration—The Low Molecular Weight Gel Filtration Calibration Kit (Amersham Biosciences) was used to calibrate a Superdex S-75 gel filtration column (Amersham Biosciences) according to the manufacturer's instructions. Briefly, 200 μl each of ovalbumin (43 kDa) and ribonuclease A (13.7 kDa) at 5 mg/ml or albumin (67 kDa) and chymotrypsinogen A (25 kDa) were loaded onto a column pre-equilibrated with S-75 buffer (20 mM Tris, pH 7.5, 150 mM NaCl, 1 mM dithiothreitol, and 2 mM calcium acetate) at 0.8 ml/min. The void volume (V_o) was determined by the elution volume of blue dextran (2000 kDa). Purified full-length CIB1 (250 μl of 4 mg/ml) was loaded onto the column that had been pre-equilibrated with 2 mM calcium acetate or 2 mM EGTA. The cytoplasmic αIIb peptide (Ac-LVLAMWKVGFFKRNRPPLEED-DEEGQ-COOH) was added to CIB1 in a molar ratio of 2:1, with 200 μl of CIB1 (65 μM) and 100 μl of αIIb (146 μM) loaded.

Analytical Ultracentrifugation—Purified full-length CIB1 was equilibrated to AUC buffer (20 mM Tris, pH 7.5, 150 mM NaCl, and either 2 mM $(CH_3COO)_2Ca$ or 2 mM EGTA) using a Vivaspin 10 MWCO concentrator (Vivascience, Hannover, Germany). The final concentrations of CIB1 were ~230, ~180, and ~80 μM, with A_{280} values of ~0.6, 0.4, and 0.2. For experiments with the cytoplasmic αIIb peptide (Ac-LVLAM-WKVGFFKRNRPPLEEDDEEGQ-COOH), a 1:1 molar ratio of αIIb to CIB1 was used. Equivalent concentrations of αIIb peptide were used in the sample and reference cells. Prior to centrifugation, impurities of the αIIb peptide were eliminated by performing a buffer exchange in a stirred cell (Amicon) with a 1,000 NMWL Ultrafiltration Membrane (Millipore) of regenerated cellulose. Analytical ultracentrifugation was performed using a Beckman Optima XL-I Ultracentrifuge, a Ti-60 rotor and a 6-sector cell (1.2-cm path length). For CIB1 protein alone, samples were centrifuged at 16,000 rpm for 26 h at 20 °C. Offset was determined by meniscus depletion by centrifugation at 45,000 rpm for 6 h. For CIB1 plus αIIb samples, centrifugation was performed at 16,000 rpm for 32 h at 20 °C, and offset was determined by centrifugation at 40,000 rpm for 8 h. Equilibrium is determined to have been reached when data collected every 2 h did not change from the previous reading. Data were fit using XL-A/XL-1 Data Analysis Software Version 4.0 (Beckman Instruments, Inc., 1997) using values of 0.736 for the partial specific volume and 1.0 for solvent density.

Data Collection—The data used for phasing by single-wavelength anomalous diffraction were collected from a single crystal of CIB1 on a Rigaku RU-H3R rotating anode x-ray generator fitted with a chromium anode and Osmic VariMax-Cr optics, which together generate CrK_α radiation (λ = 2.29 Å) and a Rigaku R-AXIS IV imaging plate area detector. Chromium K_α radiation is more suitable than CuK_α (λ = 1.54 Å) for detecting the dispersion signal from intrinsic elements such as calcium and sulfur of CIB1 protein, because the signal is doubled ($\Delta f'' = 2.51$ e⁻ and $\Delta f'' = 1.14$ e⁻, respectively) compared with that of CuK_α ($\Delta f'' = 1.29$ e⁻ and $\Delta f'' = 0.56$ e⁻, respectively). The VariMax-Cr was equipped with a slit that allowed the divergence to be tuned for the sample. This slit setting was optimized by maximizing I/σ(I) on equivalent screening images. The crystal was mounted in an arbitrary orientation, and data were collected at cryogenic temperatures in a single continuous scan. Both incident and diffracted beam helium beam paths were used to minimize air absorption and scattering. Data collection statistics are given in Table I.

For phasing, we collected 510° of data to ensure high redundancy for the calcium and sulfur anomalous signal, although with the chromium wavelength x-rays, this much redundancy is probably not necessary (25). Data were processed with HKL2000 (42), which has an absorption correction that is needed for the longer wavelength chromium x-rays (25). Due to the longer wavelength and the necessity to use the R-AXIS IV detector with a 300-mm image plate width, the crystal-to-detector distance was 122 mm, and the maximum resolution for this data set was 2.7 Å. The structure was refined against data collected from another crystal collected at the SER-CAT beamline at the Advanced Proton Source at 1.0 Å wavelength; this crystal diffracted to 2.0 Å.

Structure Determination and Refinement—Calculation of the Matthews coefficient indicated two CIB1 molecules per asymmetric unit in the $P2_1$ cell. The program SOLVE (26) was used to locate the positions of anomalous scatterers from the chromium data. We used the "single-wavelength anomalous diffraction" script (to 3.0 Å) provided on the SOLVE website to search for the eight highest peaks, reasoning that these might correspond to individual calcium ions (with a higher $\Delta f'$ at 2.2909 Å compared with sulfur) bound to each of the EF-hands in the asymmetric unit. SOLVE easily found eight sites with occupancies
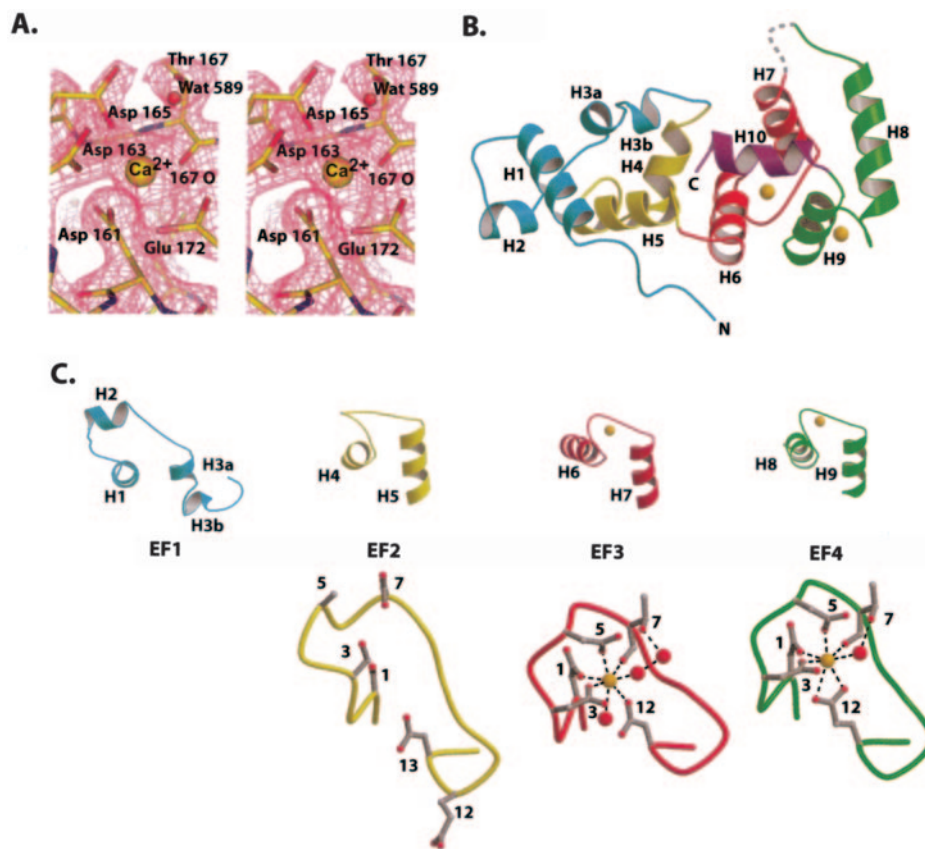
FIG. 1. **Electron density map, overall fold, and EF-hand geometry of CIB1.** *A*, electron density from EF-hand 4 in CIB1. The $2F_o - F_c$ electron density omit map (shown in *stereo*; contoured to 1 σ) was calculated by removing all atoms within 10.0 Å of the coordinating Ca^{2+} ion. Highlighted are the seven ligands that coordinate the calcium ion with a pentagonal bipyramidal geometry typical of EF-hands. Equatorial ligands include the side-chain carboxylates of Asp-161, Asp-163, Asp-165, and Glu-172 and the carbonyl oxygen (O) of Thr-167, while axial ligands are provided by the remaining oxygen of the carboxylate group of Glu-172 and a water molecule. *B*, *ribbon diagram* of the overall fold of CIB1 showing the positions of the high affinity Ca^{2+} ions (*gold spheres*) bound to EF-hands 3 and 4. Regions are *color-coded*: N-terminal region and EF1 are *blue*, EF2 is *yellow*, EF3 is *red*, EF4 is *green*, and the C-terminal helix is *purple*. Helices as well as the termini are labeled; a *dotted line* indicates the disordered loop between helices H7 and H8. *C*, *ribbon diagram* of EF-hands 1 through 4, underneath which are *worm diagrams* of the EF-hands showing individual amino acids involved in Ca^{2+} binding for EF3 and EF4, and possible Ca^{2+} binding amino acids based on their position (positions 1, 3, 5, 7, 12, and 13) in the EF2 loop. Because the conformation of EF1 is degenerate, no worm figure is shown. In this diagram, relevant protein oxygens and waters are *red*. *Dashed lines* indicate calcium ligation or hydrogen bonding.

ranging from 0.147 to 0.522. The overall Z score from SOLVE was 30.9, and the figure of merit was 0.39. Only two C-terminal EF-hands per CIB1 monomer are occupied by individual calcium ions. There are, however, two more calcium ions per CIB1 monomer that bind at surface positions and are most likely due to the high Ca^{2+} concentration (300 mM) in the crystallization medium. That gives a total of eight calcium ions in the asymmetric unit. The top eight sites found by SOLVE were not all calcium ions; three were sulfur atoms.

The program RESOLVE (27) was used to find non-crystallographic symmetry and carry out "statistical" solvent flattening. Three pairs of the eight sites were related by NCS, and the "overlap of NCS-related density" was 0.76 in RESOLVE. The solvent-flattened electron density map from RESOLVE was used to trace the chain of one of the two monomers of CIB1 in the asymmetric unit. The process was guided by the structure of calcineurin B (PDB code 1TCO), which is 57% homologous to CIB1. The sequence in the helices surrounding the EF-hands was matched easily to density; however, the density in the EF-hand loops was not as continuous and clear. An anomalous difference Fourier map using the phases from the eight SOLVE sites produced a new set of sites, which turned out to be sulfur and lower occupancy calcium atoms. The chain tracing was verified using the sulfur sites from cysteine and methionine residues. Once a preliminary model of the first molecule in the asymmetric unit was built, molecular replacement using the CCP4 program AMoRe (28) was used to position the second molecule. The independently determined positions of calcium and sulfur atoms determined by SOLVE verified this solution.

The density for the second molecule is significantly weaker, especially in the second half of the molecule that contains the two EF-hand calcium ions. The temperature factors for this molecule in initial rounds of conjugate gradient or simulated annealing refinement using CNS

(29) were quite high (average temperature factors for all atoms in molecules 1 and 2 were typically ~40 and ~70 Å², respectively). R_{free} values were just below 30% for these refinements, using either the 2.0 Å data set collected at the synchrotron, or the chromium data set to 2.8 Å. If the packing is inspected, the second molecule ("B") has fewer intermolecular contacts in the crystal, apparently giving it a more flexible position and thereby more average disorder as indicated by high temperature factors. A TLS refinement using the CCP4 program Refmac5 (43) to 2.0 Å using each subunit and its associated calcium ions as a TLS "group," and using tight geometrical restraints (matrix diagonal weighting term = 0.05), gave a model with R_{work} = 21.2% and R_{free} = 25.7%. The r.m.s. bond and angle deviations were 0.01 Å and 1.10°, respectively. From the Ramachandran plot, 2 (0.6%) and 1 residues (0.3%) were found in generously allowed and forbidden regions, respectively; however, these residues were either at the N terminus (residues 13 and 14 in molecule A) or neighboring a disordered loop (residue 146 in molecule B) where the density is poor.

Sequence Alignment—Sequences represented in Fig. 3*B* were aligned using ClustalX (30), and the output guide tree file was imported and displayed as a dendrogram using the program TreeView 1.6.6 (taxonomy.zoology.gla.ac.uk/rod/rod.html).

RESULTS AND DISCUSSION

Overall Structure of CIB1 and Geometry of Ca^{2+} Binding—Full-length CIB1 consistently yielded twinned, poorly formed crystals. Because proteins homologous to CIB1, such as recoverin, have a disordered N terminus (31), and secondary structure suggests that this region is also disordered in CIB1, CIB1 Δ1–8 was used for crystallization and structure determination.

TABLE I

Data collection and refinement

	Chromium	APS
Data collection		
Source	Chromium	APS
λ (Å)	2.29	1.00
Space group	P2$_1$	P2$_1$
Unit cell		
(Å)	56.61, 50.98, 77.13	56.66, 51.01, 77.21
(°)	90, 103.128, 90	90, 103.12, 90
Rotation range (°)	510	360
Resolution (Å)	40–2.6	40–2.0
Reflections	633,650	589,209
Unique reflections	12,013	29,442
$R(I)_{\text{merge}}$ [a] (%)	4.6 (12.6)[b]	5.8 (23.4)
Completeness (%)	94.1 (88.1)	95.4 (81.0)
Redundancy	10.4 (8.4)	7.3 (6.2)
$\langle I/\sigma(I)\rangle$	54.0 (14.5)	32 (5.8)
Data processing	HKL2000	HKL2000
Anomalous scatterers per A.U.[c]	8 Ca, 3 S	
Calculated anomalous $\langle\Delta F\rangle/\langle F\rangle$ (%)	3.7	
Refinement and model statistics		
Resolution (Å)	40–2.0	
Number of protein atoms	2781 (2 molecules/A.U.)	
Number of waters	397	
$F/\sigma(F)$ cutoff	0	
R_{cryst} [d]	21.2% (24.4)	
R_{free} [d]	25.7% (30.2)	
r.m.s.d. bonds (Å)	0.01	
r.m.s.d. angles (°)	1.10	
Ramachandran plot		
% in most favored regions	92.5	
% in additional allowed regions	6.6	
% in disallowed regions	0.3	

[a] $R(I)_{\text{merge}} = 100 \times \Sigma_{hkl}|I - \langle I\rangle|/\Sigma_{hkl}\langle I\rangle$, where I is the observed intensity and $\langle I\rangle$ is the average intensity from observations of symmetry related reflections, respectively.

[b] Values in parentheses are for the outermost resolution shell.

[c] A.U., asymmetric unit(s).

[d] R_{cryst} and $R_{\text{free}} = 100 \times \Sigma\|F_o| - |F_c\|/\Sigma|F_o|$, where 5% of the reflections were held aside for R_{free} throughout refinement.

The structure of CIB1 was solved by single-wavelength anomalous diffraction phasing using chromium radiation (λ = 2.29 Å, Rigaku/MSC Inc., The Woodlands, TX). These data were collected to 2.7 Å, but phases were eventually extended to 2.0 Å using native data sets collected both in-house and at the SER-CAT beamline at Advanced Photon Source (Argonne, IL). There are two molecules of CIB1 in the asymmetric unit. The electron density (Fig. 1*A*) has been fit with models of CIB1 encompassing residues 12–191 except for a disordered loop between residues 137 and 142 in molecule A and 136–145 in molecule B.

The overall fold of CIB1 is shown in Fig. 1*B* and is very similar to other Ca^{2+}-binding proteins containing four EF-hands, such as calmodulin and calcineurin B. However, we observed that only EF-hands 3 and 4 of CIB1 bind Ca^{2+} (Fig. 1, *B* and *C*), as previously demonstrated by NMR (5). Calcium ions bind canonical EF-hands with high affinity due to acidic residues at positions 1, 3, 5, and 12, where residues at positions 1, 3, and 5 contribute individual ligands to the coordination sphere and the residue at position 12 contributes two ligands (32). In most EF-hands, a backbone carbonyl at position 7 as well as a water molecule that is hydrogen-bonded to a side-chain oxygen from position 7 complete the coordination sphere, yielding a pentagonal bipyramidal geometry. In EF4 of CIB1 (Fig. 1*C*), the side chains of Asp-161 (position 1), Asp-163, Asp-165, and Glu-172 (position 12) coordinate Ca^{2+}, with Glu-172 being a bidentate ligand. Thr-167 (position 7) ligates Ca^{2+} through its carbonyl oxygen and also coordinates a water molecule that ligates Ca^{2+}. Similarly, in EF3 (Fig. 1*C*), the Ca^{2+} is coordinated by the side chains of Asp-116 (position 1), Asp-118, Asp-120, and Asp-127 as well as the carbonyl of Thr-122 (position 7) and two water molecules. One ligating water molecule is bridged through an additional water molecule interacting with the side chain of Thr-122, and the other ligating water

molecule is seen in only one molecule of the asymmetric unit. In EF4, this water molecule is replaced by the bidentate ligation of Glu-172 (position 12). Relative to EF4, the ligation sphere of the Ca^{2+} in EF3 is less well ordered, which is consistent with the fact that EF3 binds Ca^{2+} with a lower affinity than EF4 (5).

Calcium ions are not bound in EF1 and EF2. It is not surprising that Ca^{2+} is absent from EF1, because it has an additional eight amino acids within the loop that normally binds Ca^{2+}. Following this extended loop region in EF1, the helix that typically corresponds to the second helix in an EF-hand is kinked at Pro-62, a residue conserved in calmodulin and calcineurin B, thereby creating two smaller helices (H3a and H3b) (Fig. 1*C*). EF2 is less radically modified from a canonical EF-hand domain. For example, many of the residues (positions 1, 3, and 5) within the loop that are typically acidic and chelate calcium ions have been replaced with serine or alanine. The EF2 loop also contains 13 residues rather than 12, with the extra residue, Pro-82, inserted after position 3.

A high concentration of Ca^{2+} (300 mM calcium acetate) was necessary for crystallization, presumably explaining why each monomer of CIB1 binds an additional two Ca^{2+} ions in positions not typically associated with EF-hand domains (see Table I). There are six water molecules in the octahedral coordination sphere of each of these Ca^{2+} ions, indicating that both binding events are of low affinity and most likely not biologically relevant, which is consistent with previous binding data (5).

The helices of EF-hands reorient in relation to one another when Ca^{2+} is bound (33). The interhelical angle between the E and F helices is used as a measure of whether these helices display a Ca^{2+}-bound (open) conformation or a Ca^{2+}-free (closed) conformation. In a closed conformation, E and F helices are close to one another and the interhelical angle ($180° - \theta$) is large. In an open conformation, when Ca^{2+} is present, the E
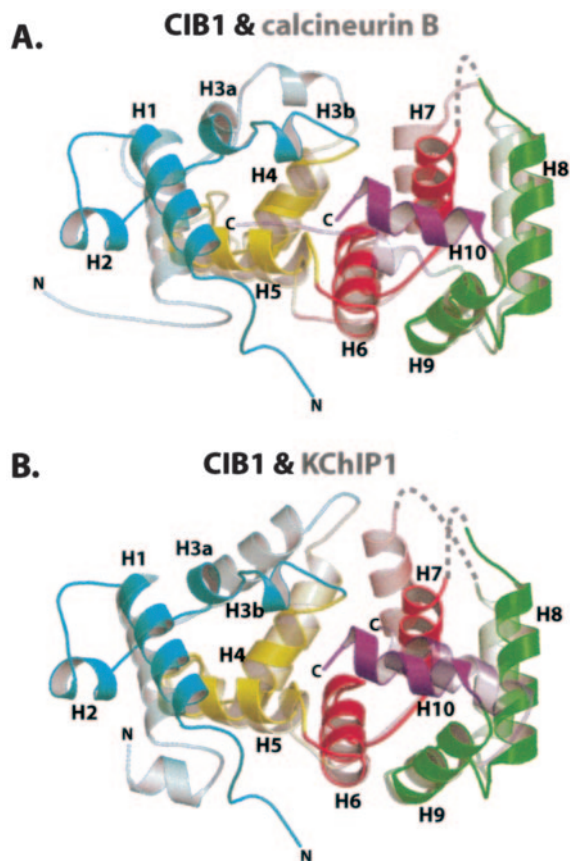
FIG. 2. **Superposition of CIB1 with its closest structural homologs.** *A*, superposition of CIB1 with calcineurin B (PDB code 1TCO) *B*, superposition of CIB1 with KChIP1 (PDB code 1S6C). N and C termini are labeled, and the different regions are *colored* according to the scheme in Fig. 1, with the *ribbons* for calcineurin B and KChIP1 being *semi-transparent*.

and F helices are typically farther apart and the interhelical angle is smaller. For example, Ca^{2+}-free calmodulin has interhelical angles between 130° and 140°, whereas Ca^{2+}-bound calmodulin has interhelical angles between 85° and 100° (23). To determine whether the EF-hands of CIB1 displayed an open or closed conformation, we calculated the interhelical angles using the program interhlx (33). EF2, EF3, and EF4 of CIB1 display similar interhelical angles, with values of 116.4°, 113.2°, and 111.5°, respectively. Because these angles are so similar, they indicate that EF2, which does not contain Ca^{2+}, adopts an open conformation like those of Ca^{2+}-bound EF3 and EF4. This open conformation is maintained by hydrogen bonds across the EF2 loop involving residues that typically bind Ca^{2+} (positions 1, 3, 7, and 13). EF1, which is highly degenerate, has an interhelical angle of 125.5°, which is indicative of a more closed conformation.

CIB1 and Its Structural Relationship to Other EF-hand-containing Proteins—To compare the structure of CIB1 to other EF-hand-containing proteins, the coordinates of CIB1 (the first molecule in the asymmetric unit) were compared with other proteins in the Protein Data Bank using MSD-fold (www.ebi. ac.uk/msd-srv/ssm/). As expected, a number of mammalian EF-hand-containing proteins showed significant homology to CIB1, the two most significant being calcineurin B (PDB code 1TCO, Z-score of 5.2, r.m.s.d. of 2.5 Å over 136 residues, 27% sequence identity) and KChIP1 (Z-score of 3.9, r.m.s.d. of 2.6 Å over 136 residues, 24% sequence identity). The structural alignment of these proteins based on the output from MSD-fold is shown in Fig. 2 (*A* and *B*). In addition to these proteins, an *Arabidopsis* protein (AtCBL2, PDB code 1UHN) (34) was found

to have strong structural homology to CIB1 (Z-score of 5.1, r.m.s.d. of 2.4 Å over 137 residues, 24% sequence identity). This protein is part of a distinct calcineurin B-like family of *Arabidopsis* proteins that interact with a novel family of plant serine/threonine protein kinases (35).

Although CIB1 closely aligns to other EF-hand-containing proteins in EF2, EF3, and EF4, significant differences appear within EF1 and the N-terminal region. As stated previously, CIB1 contains a long insertion within the EF1 loop that is not found in any of the structures of EF-hand-containing proteins solved to date, including calcineurin B and KChIP1. The geometries of helices H3a and H3b (Fig. 1*C*), including the bend of the helices due to the proline residue described previously, are recapitulated in calcineurin B (Fig. 2*A*), but not in KChIP1 (Fig. 2*B*); this proline residue causes a kink in these helices that is also conserved in calmodulin. However, due to the large insertion in the EF1 loop, helices H3a and H3b in CIB1 do not superimpose on the equivalent helices in calcineurin B, despite the similar proline-induced helical break.

The N-terminal regions of calcineurin B and NCS proteins point away from the center of the molecule, but the equivalent portion of CIB1 points to the center of the protein and forms a number of interactions with helix H5 and H6 (Fig. 2). As crystal packing interactions also occur in this region and the temperature factors for the N terminus are generally higher than in the helices of the EF-hands, it is not clear if this conformation of the N terminus is biologically significant.

Finally, the C terminus of CIB1 forms an α-helix that is similar in position to the C-terminal helix of KChIP1 (Fig. 2). Because the C terminus plays an important role in target recognition both in calcineurin B and in KChIP1, this region will be discussed in greater detail in a later section ("Potential Ligand Binding Site of CIB1").

*Sequence Alignment*—Several proteins in the sequence data base from arthropods to humans share significant sequence homology to CIB1. Three proteins in humans with high homology to CIB1 are CIB2 (also known as KIP2), CIB3 (also known as KIP3), and CIB4, which share 59%, 62%, and 64% similarity, respectively. There is currently no published data on CIB3, and only the expression profile and chromosomal location have been determined for CIB2 (36). CIB4 (NCBI accession number XP_059399) is named by the present authors based on a sequence from automated computational analysis of the human genome.

Based on the sequence alignment (Fig. 3*A*), all CIB homologs have a large insertion within EF1, strongly suggesting that this EF-hand cannot bind Ca^{2+} in any of the CIB homologs. Similarly, all CIB homologs contain a proline equivalent to Pro-62 of CIB1 that causes a kink between helices H3a and H3b (Fig. 3*A*), which is important for the overall structure of the hydrophobic binding pocket (see subsequent section). However, one notable difference among CIB homologs is that the EF2 loop (between helices H4 and H5) of CIB2 and CIB3 contains more acidic residues than CIB1, indicating that CIB2 and CIB3 may each bind an additional Ca^{2+} ion within this region. Differences in the number of bound Ca^{2+} ions among homologous proteins are not surprising, in that differences in Ca^{2+} stoichiometry are observed among members of the NCS family. For example, KChIP1 binds Ca^{2+} ions in EF-hands 3 and 4 (23), recoverin binds Ca^{2+} ions in EF-hands 2 and 3 (1), and frequenin binds Ca^{2+} ions in EF-hands 2, 3 and 4 (37).

The *dendrogram* in Fig. 3*B* depicts the sequence relatedness of CIB1 and its homologs, as well as a number of other mammalian Ca^{2+}-binding proteins. From this analysis, we conclude that CIB-like proteins, found in species from arthropods to humans, form a family distinct from both the calcineurin B-like and NCS proteins. Members of the CIB family share closest
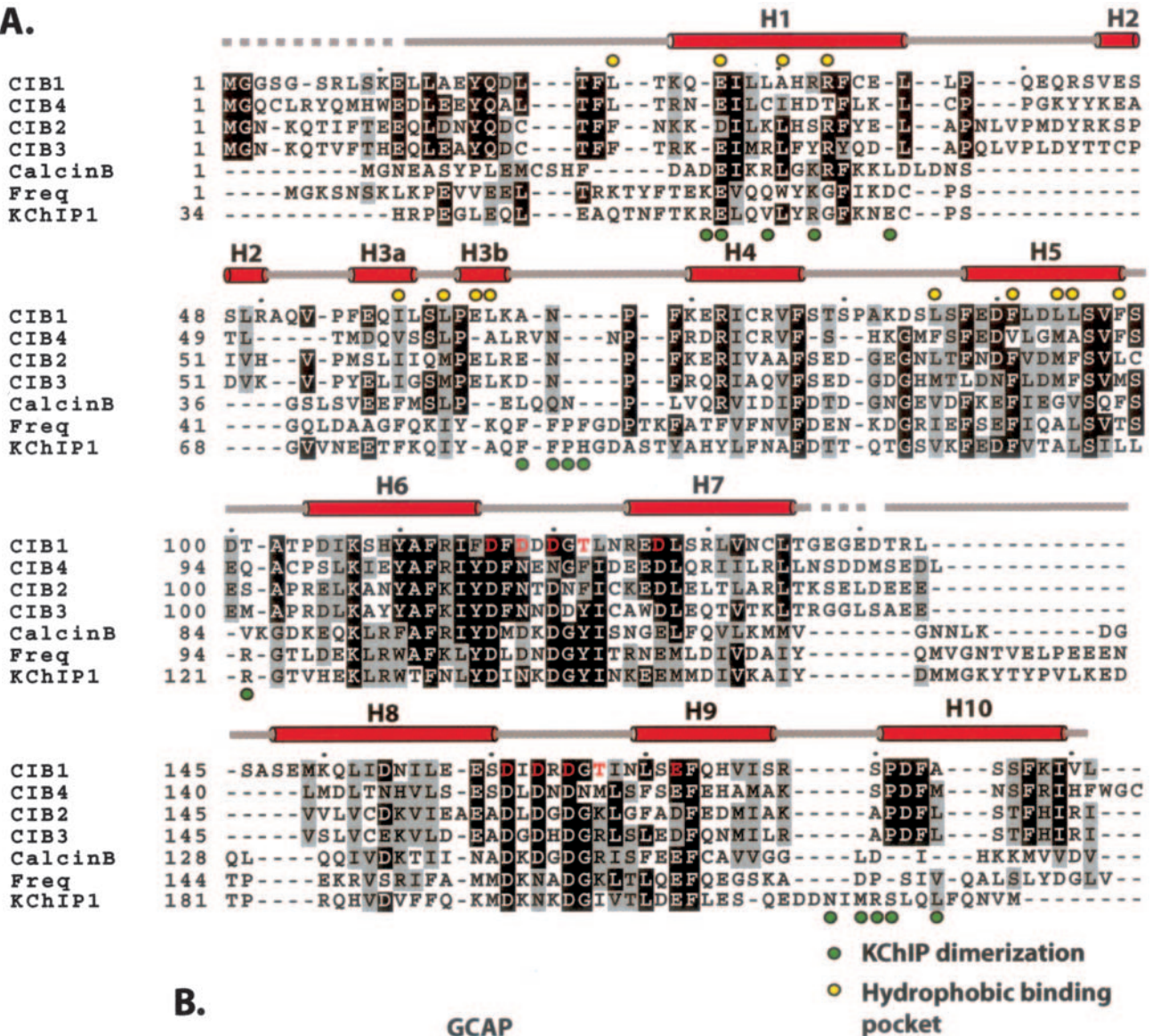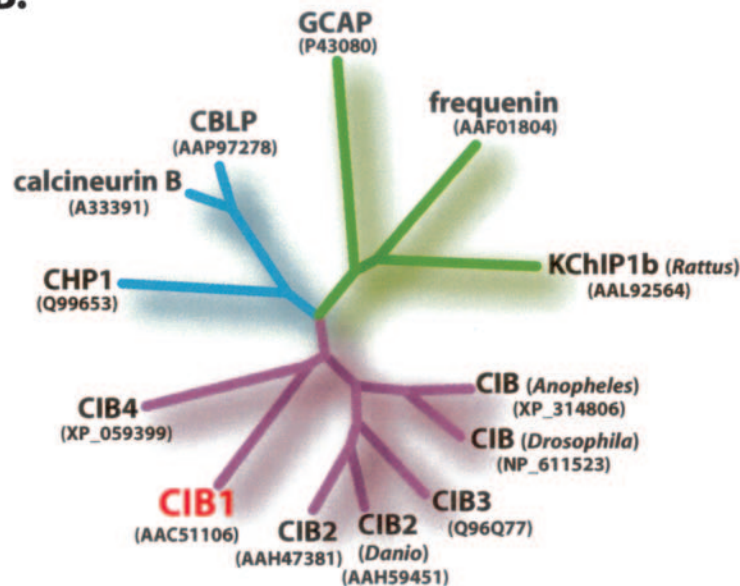
FIG. 3. **Relationship of CIB1 with some of its nearest homologs.** *A,* sequence alignment of CIB1 with its three human homologs (CIB2, CIB3, and CIB4), calcineurin B and two NCS proteins, KChIP1 and frequenin. Alignment of CIB1 with CIB2, CIB3, and CIB4 was performed using ClustalX (30) and then merged with the structural alignment from MSD-fold (www.ebi.ac.uk/msd-srv/ssm/) of CIB1 with calcineurin B (PDB code 1TCO), KChIP1 (PDB code 1S6C), and human frequenin (PDB code 1G8I). The positions of helices (*red tubes*), loop regions (*gray lines*), and disordered regions (*gray dotted lines*) in the CIB1 structure are shown above the alignment, and every tenth residue in CIB1 is marked by a *dot* above the alignment. Residues in CIB1 involved in Ca^{2+} binding are *colored red*, and residues that correspond to the CIB1 hydrophobic binding
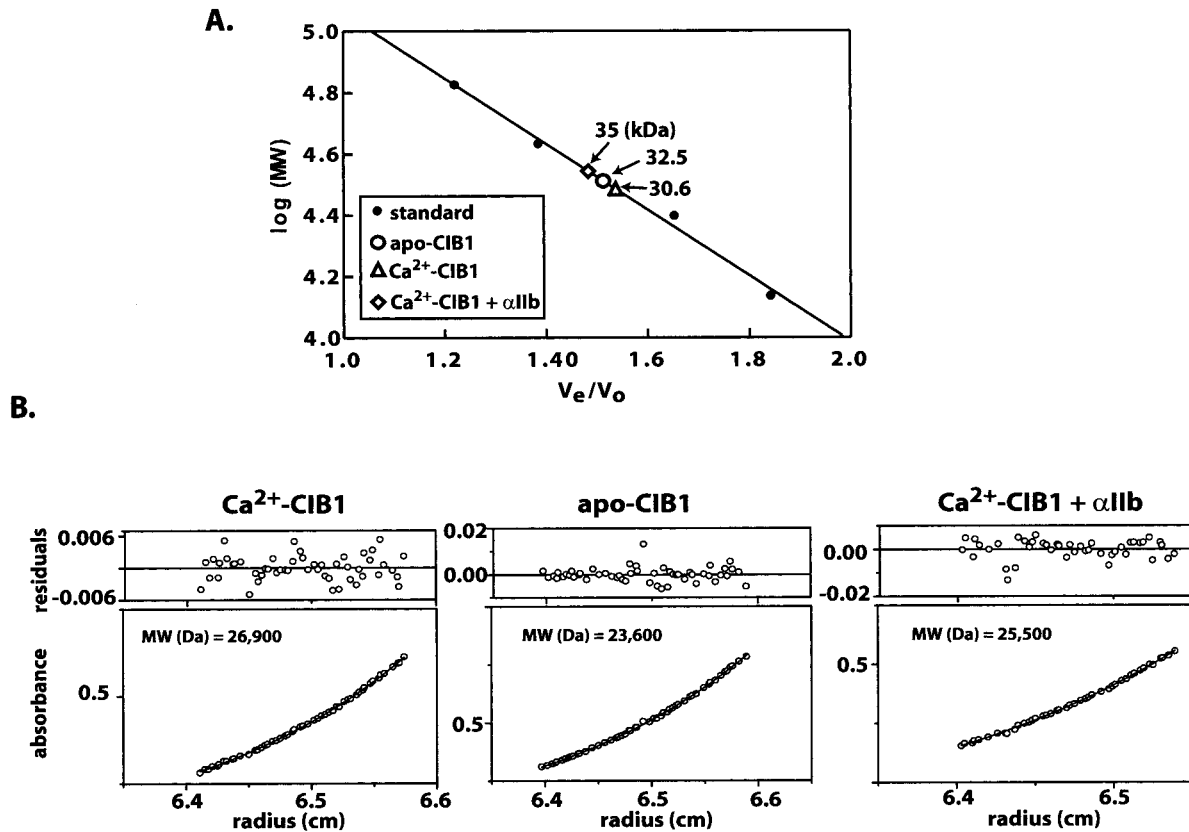
A.

B.

FIG. 4. **CIB1 primarily forms monomers in the presence or absence of Ca^{2+} and the αIIb cytoplasmic domain.** *A*, elution profiles of apo-CIB1, Ca^{2+}-CIB1, and Ca^{2+}-CIB1 plus αIIb cytoplasmic tail peptide were determined using a Superdex S-75 column (Amersham Biosciences). The molecular mass standards used were albumin (67 kDa), ovalbumin (43 kDa), chymotrypsinogen A (25 kDa), and ribonuclease A (13.7 kDa). The elution volume (V_e) of blue dextran was used to determined the void volume (V_o). *B*, sedimentation equilibrium data of Ca^{2+}-CIB1, apo-CIB1, and Ca^{2+}-CIB1 plus αIIb by analytical ultracentrifugation. Molecular weights fit using a one-state model are posted on each graph.

homology to calcineurin B and its relatives, but sequence homology is still quite low between CIB family members and calcineurin B (~30% sequence identity). Among the four human CIB proteins, CIB2 and CIB3 are more ancestral, because CIB proteins from *Drosophila melanogaster*, *Anopheles gambiae*, and *Danio rerio* more strongly resemble these proteins.

Oligomeric State of CIB1—Many NCS homologs of CIB1 form dimers or tetramers under various conditions. For instance, KChIP3 tends to form tetramers at protein concentrations higher than 20 μM and stable dimers at low protein concentrations (38). Similarly, neurocalcin forms a dimer in the crystal (39) and in solution when Ca^{2+} is present (40) but forms a monomer when Ca^{2+} is absent (40). Conversely, GCAP-2 forms dimers in the absence of Ca^{2+} and monomers in the presence of Ca^{2+} (40). Also, unmyristoylated recoverin forms a dimer within the asymmetric unit of the crystal structure (31), whereas KChIP1 also forms dimers, but only in the presence of ligand (23). Residues involved in KChIP1 dimerization are poorly conserved in CIB1 (Fig. 3*A*).

To determine whether CIB1 forms oligomers in the presence or absence of Ca^{2+} and ligand, we first performed gel filtration (Fig. 4*A*). In the presence of Ca^{2+}, CIB1 eluted at a volume corresponding to 30.6 kDa, which is larger than its molecular mass of 21.7 kDa, but smaller than the expected size of a dimer, which would be 43.4 kDa (Fig. 4*A*). The anomalous elution volume of CIB1 may be accounted for by the fact that gel

filtration columns are typically calibrated using spherical proteins as standards, while EF-hand-containing proteins have a more oblong "dumbbell-shape." Similarly, GCAP-2, which has a molecular mass of 23.8 kDa, exhibits an anomalous elution volume, with the monomer eluting at 30.6 kDa and the dimer eluting at 57 kDa (40). Apo-CIB1, or CIB1 in the absence of Ca^{2+}, elutes at 32.5 kDa, consistent with NMR data of apo-CIB1, which displays a conformation that is more extended than that of Ca^{2+}-CIB1 (5). An extended conformation is also seen in Ca^{2+}-free recoverin, as opposed to its more compact conformation when Ca^{2+} is present (1). Ca^{2+}-CIB1 in the presence of the entire αIIb cytoplasmic peptide eluted at 35 kDa, which is representative of the molecular mass of monomeric CIB1 plus the molecular mass of the peptide (3.1 kDa).

To confirm the gel filtration results, we performed sedimentation equilibrium of purified recombinant full-length CIB1 in the presence of either 2 mM (CH$_3$COO)$_2$Ca or 2 mM EGTA by analytical ultracentrifugation (AUC). These experiments were also performed in the presence of the αIIb peptide, with high, medium, and low concentrations of CIB1 as described under "Experimental Procedures." Molecular weight determinations are given for the intermediate concentration (150–190 μM), and the other concentrations give similar results. The AUC data fit to a molecular mass for Ca^{2+}-CIB1 of 26.9 kDa compared with a calculated value of 21.7 kDa, with an offset of 0.05 (Fig. 4*B*). This indicates an equilibrium favoring monomers with the

pocket (see Fig. 5) and that are involved in dimerization in rat KChIP1 (PDB code 1SC6) are highlighted with *brown* and *green circles*, respectively. *B*, evolutionary relationship of CIB1 with other Ca^{2+}-binding proteins. The *dendrogram* (derived as described under "Experimental Procedures") is colored to highlight the distinct families of CIB-like proteins (*purple*), calcineurin B-like proteins (*blue*), and NCS proteins (*green*). The proteins are human unless otherwise stated, and their NCBI accession numbers are included.

CIB1

KChIP1 / Kv4.2 (1–30)

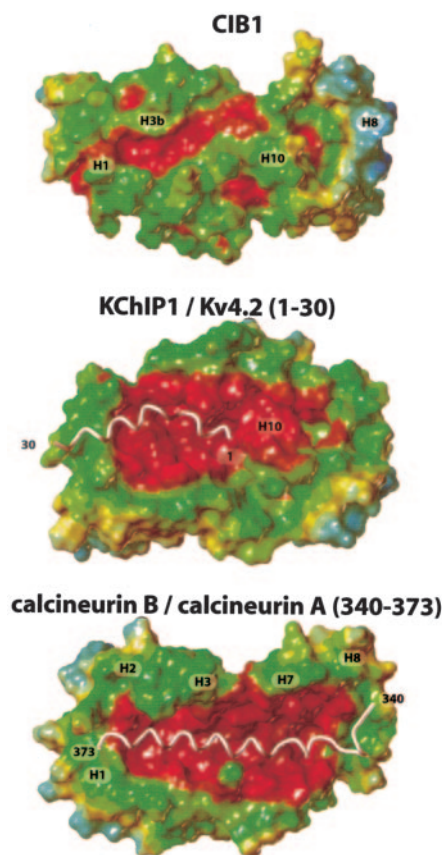**calcineurin B / calcineurin A (340–373)**

FIG. 5. **CIB1 contains a strongly hydrophobic channel that is preserved in other EF-hand-containing proteins.** Coordinates for CIB1 (PDB code 1XO5), calcineurin B (PDB code 1TCO), and KChIP1 (PDB code 1S6C) were read by the program SYBYL version 6.9.1 (www.tripos.com), hydrogens were added, and MOLCAD molecular surfaces were generated and colored to represent the spectrum of hydrophobic potential (*red*, highly hydrophobic; *blue*, highly hydrophilic). The orientation of CIB1 in this molecular surface representation is very similar to that in Fig. 1*B*. The region of calcineurin A in contact with calcineurin B, as well as the Kv4.2 peptide, are shown as helical worms in the binding sites of calcineurin B and KChIP1, respectively, and their boundaries are enumerated. Positions of the C termini of CIB1, calcineurin B, and KChIP1 on these surfaces are labeled, as are selected secondary structural elements.

ability to form dimers for a small percentage of molecules. The molecular mass from AUC for apo-CIB1 was 23.6 kDa, with an offset of -0.021, indicating a population almost entirely monomeric. To determine whether Ca^{2+}-CIB1 forms dimers in the presence of ligand, we performed experiments with equivalent concentrations of αIIb peptide in the sample and reference cells. The molecular mass determined from AUC was 25.5 kDa (offset of -0.255), compared with a calculated molecular mass for a 1:1 CIB1-peptide complex of 24.8 kDa, indicating the prevalence of a 1:1 complex of CIB1 and αIIb. The high offset values obtained for experiments with αIIb are indicative of the difficulty in precisely matching the αIIb concentration in the reference and sample cells. Taken together, these data indicate that CIB1, unlike NCS proteins, remains monomeric in the presence and absence of Ca^{2+} and ligand.

Potential Ligand Binding Site of CIB1—EF-hand-containing proteins contain hydrophobic pockets that bind the amphipathic α-helices of their ligands. These binding pockets exist on the opposite side of the molecule from the Ca^{2+}-binding sites of EF-hands 3 and 4. In Fig. 5, the molecular surfaces of CIB1, KChIP1, and calcineurin B are colored by hydrophobic potential, and the positions of the portions of calcineurin A and Kv4.2 bound in calcineurin B and KChIP1, respectively, are traced.

Residues within the hydrophobic binding pocket of CIB1 are denoted in the sequence alignment on Fig. 3*A*.

In the case of calcineurin B, calcineurin A binds in a hydrophobic channel formed from residues in helices H1, H2, H3, and H7 (equivalent to H1, H3, H4, and H8 in CIB1) and the C-terminal region (see Fig. 5) (22). In KChIP1, the Kv4.2 peptide binds as a continuation of the C-terminal helix H10 in a hydrophobic channel formed by EF1 and EF2 (23). Helix H10 of KChIP1 is in a similar position to the C-terminal helix of CIB1. Similarly placed hydrophobic channels have been found in other NCS proteins (37, 39, 41), although structures of these proteins with their ligands have not yet been reported.

CIB1 contains a large hydrophobic channel just following the C terminus of the molecule, as in KChIP1, but the binding pocket is considerably narrower than that of KChIP1. This is in part due to the bend at Pro-61 and the associated position of helix H3b, which pushes further into the hydrophobic binding pocket relative to the similar helix in KChIP1. Binding studies have shown that CIB1 binds to a minimal 15-amino acid region of integrin αIIb (7), which corresponds to four α-helical turns. This channel ($\sim$18 Å across) would be too small to bind four turns of an α-helix ($>$25 Å). However, this hydrophobic channel continues, albeit in a narrower form, on either side of the H10 helix, so residues within this C-terminal helix could also be important in peptide binding. Indeed, it has been demonstrated that residues within this C-terminal helix (17) are critical for CIB1 binding to the αIIb cytoplasmic tail. In addition, prior to this structure, a homology model of CIB1 was generated (7) based on the structure of calcineurin B bound to calcineurin A (PDB code 1TCO). Based on this model, four residues (Leu-115, Leu-131, Ile-153, and Phe-173) were mutated and found to affect αIIb integrin binding without grossly affecting the CIB1 structure (as measured by circular dichroism). In our structure, these residues are buried under helix H10 and are thus not surface-accessible. However, loss of integrin binding via these mutations may be explained by their causing local movements of helix H10, which then would affect the structure of the hydrophobic binding groove. Another possibility is that upon integrin binding, helix H10 undergoes a conformational change such that a larger ligand binding groove is formed. In the structure of the *Arabidopsis* EF-hand-containing protein AtCLB2 (34), the C terminus completely covers the hydrophobic binding groove, and consequently it has been suggested that, upon ligand binding, the C terminus is released from this groove. For CIB1, these studies indicate the importance of the hydrophobic binding groove and the H10 helix. Additional structural and mutational studies will aid in further defining the role of this region in CIB1 binding to effectors.

In conclusion, the crystal structure of CIB1 reveals significant structural similarity to other EF-hand-containing proteins and confirms that only EF-hands 3 and 4 bind Ca^{2+} through canonical interactions characteristic of EF-hand domains. The major differences between CIB1 relative to the NCS and calcineurin B families are in the overall structure of EF1 and the N-terminal portions. The position of the C-terminal helix of CIB1 is similar to that of KChIP1, and like KChIP1, CIB1 contains a hydrophobic binding pocket near this helix. This hydrophobic binding pocket is likely to bind αIIb and possibly other targets; as shown previously, residues within this area are critical for binding αIIb (7). A family of proteins related to CIB1 has been discovered that is distinct from its closest homologs, calcineurin B and the NCS protein family. Future structural studies of CIB1 and CIB-family members with high affinity binding peptides from target proteins such as integrin

αIIb, in combination with further biochemical and cellular assays, will extend our understanding of the role of this family of proteins in cellular signaling.

REFERENCES

1. Ames, J. B., Ishima, R., Tanaka, T., Gordon, J. I., Stryer, L., and Ikura, M. (1997) *Nature* **389,** 198–202
2. Braunewell, K. H., and Gundelfinger, E. D. (1999) *Cell Tissue Res.* **295,** 1–12
3. Senin, I. I., Koch, K. W., Akhtar, M., and Philippov, P. P. (2002) *Adv. Exp. Med. Biol.* **514,** 69–99
4. Burgoyne, R. D., and Weiss, J. L. (2001) *Biochem. J.* **353,** 1–12
5. Yamniuk, A. P., Nguyen, L. T., Hoang, T. T., and Vogel, H. J. (2004) *Biochemistry* **43,** 2558–2568
6. Stabler, S. M., Ostrowski, L. L., Janicki, S. M., and Monteiro, M. J. (1999) *J. Cell Biol.* **145,** 1277–1292
7. Barry, W. T., Boudignon-Proudhon, C., Shock, D. D., McFadden, A., Weiss, J. M., Sondek, J., and Parise, L. V. (2002) *J. Biol. Chem.* **277,** 28877–28883
8. Tanaka, T., Ames, J. B., Harvey, T. S., Stryer, L., and Ikura, M. (1995) *Nature* **376,** 444–447
9. Shock, D. D., Naik, U. P., Brittain, J. E., Alahari, S. K., Sondek, J., and Parise, L. V. (1999) *Biochem. J.* **342,** 729–735
10. Haataja, L., Kaartinen, V., Groffen, J., and Heisterkamp, N. (2002) *J. Biol. Chem.* **277,** 8321–8328
11. Naik, U. P., Patel, P. M., and Parise, L. V. (1997) *J. Biol. Chem.* **272,** 4651–4654
12. Wu, X., and Lieber, M. R. (1997) *Mutat. Res.* **385,** 13–20
13. Kauselmann, G., Weiler, M., Wulff, P., Jessberger, S., Konietzko, U., Scafidi, J., Staubli, U., Bereiter-Hahn, J., Strebhardt, K., and Kuhl, D. (1999) *EMBO J.* **18,** 5528–5539
14. Hollenbach, A. D., McPherson, C. J., Lagutina, I., and Grosveld, G. (2002) *Biochim. Biophys. Acta* **1574,** 321–328
15. Ma, S., Liu, M. A., Yuan, Y. L., and Erikson, R. L. (2003) *Mol. Cancer Res.* **1,** 376–384
16. Yuan, W., McFadden, A., Wang, Z., Larsen, M. K., Boudignon-Proudhon, C., and Parise, L. V. (2003) *Blood* **102,** 160A (Abstr. 555)
17. Tsuboi, S. (2002) *J. Biol. Chem.* **277,** 1919–1923
18. Naik, U. P., and Naik, M. U. (2003) *Blood* **102,** 1355–1362
19. Naik, M. U., and Naik, U. P. (2003) *Blood* **102,** 3629–3636
20. Hwang, P. M., and Vogel, H. J. (2000) *J. Mol. Recognit.* **13,** 83–92
21. Adair, B. D., and Yeager, M. (2002) *Proc. Natl. Acad. Sci. U. S. A.* **99,** 14059–14064
22. Griffith, J. P., Kim, J. L., Kim, E. E., Sintchak, M. D., Thomson, J. A., Fitzgibbon, M. J., Fleming, M. A., Caron, P. R., Hsiao, K., and Navia, M. A. (1995) *Cell* **82,** 507–522
23. Zhou, W., Qian, Y., Kunjilwar, K., Pfaffinger, P. J., and Choe, S. (2004) *Neuron* **41,** 573–586
24. Parks, T. D., Howard, E. D., Wolpert, T. J., Arp, D. J., and Dougherty, W. G. (1995) *Virology* **210,** 194–201
25. Yang, C., Pflugrath, J. W., Courville, D. A., Stence, C. N., and Ferrara, J. D. (2003) *Acta Crystallogr. D Biol. Crystallogr.* **59,** 1943–1957
26. Terwilliger, T. C., and Berendzen, J. (1999) *Acta Crystallogr. D Biol. Crystallogr.* **55,** 849–861
27. Terwilliger, T. C. (2000) *Acta Crystallogr. D Biol. Crystallogr.* **56,** 965–972
28. Collaborative Computational Project Number 4 (1994) *Acta Crystallogr. D Biol. Crystallogr.* **50,** 760–763
29. Brunger, A. T., Adams, P. D., Clore, G. M., DeLano, W. L., Gros, P., Grosse-Kunstleve, R. W., Jiang, J. S., Kuszewski, J., Nilges, M., Pannu, N. S., Read, R. J., Rice, L. M., Simonson, T., and Warren, G. L. (1998) *Acta Crystallogr. D Biol. Crystallogr.* **54,** 905–921
30. Thompson, J. D., Gibson, T. J., Plewniak, F., Jeanmougin, F., and Higgins, D. G. (1997) *Nucleic Acids Res.* **25,** 4876–4882
31. Flaherty, K. M., Zozulya, S., Stryer, L., and McKay, D. B. (1993) *Cell* **75,** 709–716
32. Michiels, J., Xi, C., Verhaert, J., and Vanderleyden, J. (2002) *Trends Microbiol.* **10,** 87–93
33. Yap, K. L., Ames, J. B., Swindells, M. B., and Ikura, M. (2002) *Methods Mol. Biol.* **173,** 317–324
34. Nagae, M., Nozawa, A., Koizumi, N., Sano, H., Hashimoto, H., Sato, M., and Shimizu, T. (2003) *J. Biol. Chem.* **278,** 42240–42246
35. Kudla, J., Xu, Q., Harter, K., Gruissem, W., and Luan, S. (1999) *Proc. Natl. Acad. Sci. U. S. A.* **96,** 4718–4723
36. Seki, N., Hattori, A., Hayashi, A., Kozuma, S., Ohira, M., Hori, T., and Saito, T. (1999) *Biochim. Biophys. Acta* **1444,** 143–147
37. Bourne, Y., Dannenberg, J., Pollmann, V., Marchot, P., and Pongs, O. (2001) *J. Biol. Chem.* **276,** 11949–11955
38. Osawa, M., Tong, K. I., Lilliehook, C., Wasco, W., Buxbaum, J. D., Cheng, H. Y., Penninger, J. M., Ikura, M., and Ames, J. B. (2001) *J. Biol. Chem.* **276,** 41005–41013
39. Vijay-Kumar, S., and Kumar, V. D. (1999) *Nat. Struct. Biol.* **6,** 80–88
40. Olshevskaya, E. V., Ermilov, A. N., and Dizhoor, A. M. (1999) *J. Biol. Chem.* **274,** 25583–25587
41. Ames, J. B., Dizhoor, A. M., Ikura, M., Palczewski, K., and Stryer, L. (1999) *J. Biol. Chem.* **274,** 19329–19337
42. Otwinowski, Z., and Minor, W. (1997) *Methods Enzymol.* **276,** 307–326
43. Pannu, N. J., Murshidov, G. N., Dodson, E. J., and Read, R. J. (1998) *Acta Crystallogr. D Biol. Crystallogr.* **54,** 1285–1294